

See discussions, stats, and author profiles for this publication at: <http://www.researchgate.net/publication/216690549>

Tetranuclear grid-like copper(II) complexes with pyrazolate bridges: Syntheses, structures, magnetic and EPR spectroscopic properties

ARTICLE *in* JOURNAL OF THE CHEMICAL SOCIETY DALTON TRANSACTIONS · FEBRUARY 1999

Impact Factor: 4.1 · DOI: 10.1039/A807599I

CITATIONS

54

READS

23

13 AUTHORS, INCLUDING:



Eleftheria Psillakis

Technical University of Crete

84 PUBLICATIONS 3,251 CITATIONS

[SEE PROFILE](#)



Federico Totti

University of Florence

52 PUBLICATIONS 1,066 CITATIONS

[SEE PROFILE](#)

Tetranuclear grid-like copper(II) complexes with pyrazolate bridges: syntheses, structures, magnetic and EPR spectroscopic properties

Karen L. V. Mann,^a Eleftheria Psillakis,^a John C. Jeffery,^a Leigh H. Rees,^a Nicholas M. Harden,^a Jon A. McCleverty,^{*a} Michael D. Ward,^{*a} Dante Gatteschi,^b Federico Totti,^b Frank E. Mabbs,^c Eric J. L. McInnes,^c Peter C. Riedi^d and Graham M. Smith^d

^a School of Chemistry, University of Bristol, Cantock's Close, Bristol, UK BS8 1TS.
E-mail: mike.ward@bristol.ac.uk

^b Department of Chemistry, University of Florence, Via Maragliano 75177, 50144 Florence, Italy

^c EPSRC cwEPR Service Centre, Chemistry Department, University of Manchester, Manchester, UK M13 9PL

^d Department of Physics and Astronomy, University of St Andrews, North Haugh, St Andrews, Fife, UK KY16 9SS

Received 30th September 1998, Accepted 30th November 1998

Reaction of 3-(2-pyridyl)pyrazole (HL¹) and 6-(3-pyrazolyl)-2,2'-bipyridine (HL²) with nickel(II) and zinc(II) salts afforded the simple mononuclear pseudo-octahedral complexes [M(HL¹)₃][PF₆]₂ and [M(HL²)₂][PF₆]₂ respectively (M = Ni or Zn) in which the ligands co-ordinate as neutral mononucleating chelates in the same manner as *e.g.* 2,2'-bipyridine or 2,2':6',2''-terpyridine respectively. However with Cu^{II} the complexes [Cu₄(L¹)₆(solv)₂][PF₆]₂ (solv = dmf or MeOH) and [Cu₄(L²)₄(dmf)₄][PF₆]₄ were isolated and crystallographically characterised, in all cases containing four tetragonally elongated square-pyramidal copper(II) ions which are linked by pyrazolate bridges from the now deprotonated ligands L¹ and L². The approximate orthogonality of the different ligands within each complex and the approximately square array of metal ions result in a grid-like structure. In [Cu₄(L¹)₆(solv)₂][PF₆]₂ there are successively two, one, two and one pyrazolate bridges between adjacent copper(II) ions around the Cu₄ square resulting in two clearly different magnetic coupling pathways; in [Cu₄(L²)₄(dmf)₄][PF₆]₄ however, which has approximate S₄ symmetry, each Cu...Cu edge has a single pyrazolate bridge and the coupling pathways are all virtually equivalent. Prolonged drying of these compounds resulted in loss of the axial dmf ligands to give [Cu₄(L¹)₆][PF₆]₂ and [Cu₄(L²)₄][PF₆]₄. Magnetic susceptibility studies on these showed the presence of two antiferromagnetic exchange pathways for [Cu₄(L¹)₆][PF₆]₂ with *J* > 172 cm⁻¹ and *J'* < 155 cm⁻¹ (strong correlation between the parameters precludes a more precise determination), but only one antiferromagnetic exchange pathway for [Cu₄(L²)₄][PF₆]₄ with *J* = 63.5 cm⁻¹, consistent with the crystal structures of the dmf adducts. The EPR spectra of [Cu₄(L¹)₆][PF₆]₂ and [Cu₄(L²)₄][PF₆]₄ at a variety of frequencies and temperatures can be well simulated as arising from triplet species; however the spectrum of [Cu₄(L¹)₆][PF₆]₂ also contains a feature which may be ascribed to the expected thermally populated quintet state.

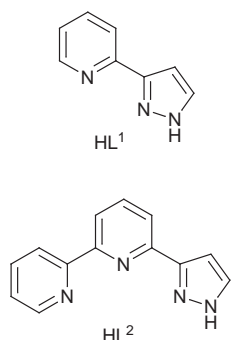
Introduction

Self-assembly processes involving carefully designed multidentate ligands and metal ions with appropriate stereo-electronic preferences can lead to the efficient and specific formation of architecturally highly sophisticated polynuclear complexes such as molecular helicates, grids, rings and boxes.¹ Although in the first instances many of these structures arose by chance, recently a systematic attempt has been made to determine the relationship between the number, type and spatial disposition of binding sites on the ligand, and the stereo-electronic preferences of the metal ion, which would allow a considerable degree of control to be exerted over the nature of the structure.² The major interest so far in these types of coordination complex has been in their remarkable structures and the specific self-assembly processes which lead to them. However there is also considerable scope for the study of metal-metal interactions in complexes where several metal ions are assembled in a well defined spatial array linked by suitable bridging ligands to mediate the interaction.³ Electrochemical properties⁴ and magnetic⁵ exchange interactions have been

extensively studied between pairs of metal ions in dinuclear complexes, and the magnetic properties of one-dimensional chain-like complexes⁵ and high-nuclearity clusters⁶ have recently been of considerable interest for the development of new magnetic materials.

In this paper we describe the syntheses, structural characterisation, and magnetic and EPR spectroscopic properties of some unusual grid-like⁷ tetranuclear copper(II) complexes prepared from simple multidentate chelating ligands HL¹ and HL² containing pyridyl and pyrazolyl donors which act as bridges *via* deprotonated pyrazole groups. The assembly of these structures is driven by the stereo-electronic requirement of the copper(II) ion for an elongated tetragonal (as opposed to regular octahedral) geometry. The preferences of Cu^I and Ag^I for four-co-ordinate geometry, of most first-row transition-metals for octahedral geometry, and of lanthanides for nine-co-ordinate geometry have all been exploited in the assembly of multinuclear complexes by self-assembly methods.¹ These new complexes represent a rare example⁸ of the exploitation of the unusual structural preference of Cu^{II} to direct self-assembly reactions and, to emphasise the point, complexes of the same

ligands with other first-row transition metal ions, having much simpler structures, are also described. The resultant grid-like copper(II) complexes contain arrays of four copper(II) ions linked by pyrazolate bridges which are known to be effective mediators of magnetic exchange interactions;^{9,10} accordingly, detailed magnetic susceptibility and EPR spectroscopic studies on these complexes are also described. A preliminary communication describing part of this work has been published.¹¹



Experimental

General details

3-(2-Pyridyl)pyrazole (HL¹)¹² and 6-(3-pyrazolyl)-2,2'-bipyridine (HL²)¹³ were prepared according to the published methods. Fast-atom bombardment (FAB) mass spectra were recorded on a VG-Autospec, using 3-nitrobenzyl alcohol as matrix, and electrospray (ES) mass spectra on a VG-Quattro instrument.

Syntheses

[M(HL¹)₃][PF₆]₂ (M = Ni or Zn). A mixture of the appropriate metal(II) acetate hydrate and HL¹ in a 3:1 molar ratio in methanol was stirred to give a clear solution, from which a solid precipitated on addition of aqueous NH₄PF₆. The solids were filtered off and dried *in vacuo* to give the desired products in 60–80% yield. Recrystallisation of both complexes from MeCN–diethyl ether afforded X-ray quality crystals.

Data for [Ni(HL¹)₃][PF₆]₂: ES MS [*m/z* (relative peak intensity, assignment)] 638 [5, {Ni(HL¹)₃(PF₆)₃}⁺], 492 [15, {Ni(HL¹)₂(L¹)₂}⁺], 347 [100, {Ni(HL¹)(L¹)₂}⁺] and 247 [1%, {Ni(L¹)₃}²⁺] {Found: C, 35.5; H, 3.0; N, 15.3. Required for [Ni(HL¹)₃][PF₆]₂·H₂O: C, 35.9; H, 2.9; N, 15.7%}.

Data for [Zn(HL¹)₃][PF₆]₂: FAB MS [*m/z* (relative peak intensity, assignment)]: 580 [4, {Zn₂(HL¹)(L¹)₂F}], 560 [12, {Zn₂(L¹)₃}], 498 [6, {Zn(L¹)(HL¹)₂}] and 353 [100%, {Zn(HL¹)(L¹)₂}] {Found: C, 35.5; H, 2.8; N, 15.5. Required for [Zn(HL¹)₃][PF₆]₂·H₂O: C, 35.6; H, 2.8; N, 15.6%}.

[Cu₄(L¹)₆(dmf)₂][PF₆]₂. A mixture of HL¹ and Cu(O₂CCH₃)₂·H₂O in a 3:2 molar ratio in MeOH was stirred for a few minutes at room temperature to afford a dark green solution. Addition of an excess of aqueous KPF₆ afforded a green precipitate which was filtered off and dried *in vacuo*. The complex was crystallised by slow diffusion of diethyl ether vapour into a concentrated solution of the crude material in dmf. X-Ray quality green crystals resulted in *ca.* 80% yield. FAB MS [*m/z* (relative peak intensity, assignment)]: 1260 {1, Cu₄(L¹)₇}; 1135 {9, Cu₄(L¹)₆F}; 993 {11, Cu₄(L¹)₅F}; 972 {9, Cu₄(L¹)₅}; 847 {15, Cu₄(L¹)₄F}; 828 {8, Cu₄(L¹)₄}; 784 {85, Cu₃(L¹)₄F}; 765 {100, Cu₃(L¹)₄}; 684 {30, Cu₄(L¹)₃}; 640 {40, Cu₃(L¹)₃F} and 621 {70%, Cu₃(L¹)₃} and numerous smaller fragments (peak masses quoted for ⁶³Cu; the isotopic patterns were consistent with the given formulations) {Found: C, 42.1; H, 3.1; N, 18.1. Required for [Cu₄(L¹)₆(dmf)₂][PF₆]₂: C, 41.7; H, 3.2; N, 18.0%}. After oven drying (70 °C) overnight the two dmf ligands were lost, as shown by IR spectroscopy (see Results and discussion) and

elemental analysis {Found: C, 41.2; H, 2.7; N, 18.0. Required for [Cu₄(L¹)₆][PF₆]₂: C, 40.7; H, 3.0; N, 17.8%}.

[Cu₄(L¹)₆(MeOH)₂][PF₆]₂. Crystals of this compound appeared when the crude tetranuclear complex, prepared as above, was crystallised from methanol by diffusion of ether vapour into the solution. The FAB mass spectrum was essentially identical to that of the dmf adduct above {Found: C, 40.4; H, 2.9; N, 16.7. Required for [Cu₄(L¹)₆(MeOH)₂][PF₆]₂: C, 40.7; H, 3.0; N, 17.1%}.

[M(HL²)₂][PF₆]₂ (M = Ni or Zn). A mixture of HL² (0.060 g, 0.27 mmol) and the appropriate metal(II) acetate hydrate (0.14 mmol) in methanol (10 cm³) was stirred at room temperature to give a clear solution, from which a solid precipitated on addition of aqueous NH₄PF₆. The solids were filtered off, dried and recrystallised from MeCN–ether to give microcrystalline powders in 70–80% yield.

Data for [Ni(HL²)₂][PF₆]₂: ES MS [*m/z* (relative peak intensity, assignment)] 501 [100, {Ni(HL²)(L²)₂}⁺], 279 [60, {Ni(L²)₂}⁺] and 251 [90%, {Ni(HL²)₂}²⁺] {Found: C, 38.6; H, 2.3; N, 14.2. Required for [Ni(HL²)₂][PF₆]₂: C, 39.3; H, 2.5; N, 14.1%}.

Data for [Zn(HL²)₂][PF₆]₂: ES MS [*m/z* (relative peak intensity, assignment)] 508 [100, {Zn(HL²)(L²)₂}⁺], 286 [35, {Zn(L²)₂}⁺] and 254 [40%, {Zn(HL²)₂}²⁺] {Found: C, 38.5; H, 2.4; N, 13.7. Required for [Ni(HL²)₂][PF₆]₂: C, 39.0; H, 2.5; N, 14.0%}.

[Cu₄(L²)₄(dmf)₄][PF₆]₄. A mixture of HL² (0.060 g, 0.27 mmol) and Cu(O₂CCH₃)₂·H₂O (0.088 g, 0.44 mmol) in MeOH (20 cm³) was stirred at room temperature until a clear blue-green solution was obtained. Addition of aqueous NH₄PF₆ afforded a blue-green precipitate which was filtered off, washed with water, and dried. Crystallisation from dmf–ether (as above) afforded a crystalline precipitate of [Cu₄(L²)₄(dmf)₄][PF₆]₄ in 50% yield. ES MS [*m/z* (relative peak intensity, assignment)]: 714 [8, {Cu₄(L²)₄(PF₆)₂}²⁺] and 284 [100%, {Cu₄L₄}⁴⁺] {Found: C, 36.6; H, 2.4; N, 13.2. Required for [Cu₄(L²)₄][PF₆]₄: C, 36.6; H, 2.1; N, 13.0% (*i.e.* the elemental analysis on the vacuum-dried crystals is consistent with loss of the co-ordinated dmf molecules, see Results and discussion)}.

X-Ray crystallographic studies

Suitable crystals were quickly transferred from the mother liquor to a stream of cold N₂ on a Siemens SMART diffractometer fitted with a CCD-type area detector. In all cases data were collected at –100 °C using graphite-monochromatised Mo-K α radiation. A detailed experimental description of the methods used for data collection and integration using the SMART system has been published.¹⁴ Table 1 contains a summary of the crystal parameters, data collection and refinement. In all cases the structures were solved by conventional direct methods and refined by the full-matrix least-squares method on all *F*² data using the SHELXTL 5.03 package on a Silicon Graphics Indy computer.¹⁵ Non-hydrogen atoms were refined with anisotropic thermal parameters; hydrogen atoms were included in calculated positions and refined with isotropic thermal parameters riding on those of the parent atom.

The complexes [M(HL¹)₃][PF₆]₂·H₂O (M = Ni or Zn; Fig. 1) are isostructural and isomorphous, and have no imposed symmetry. Both [Cu₄(L¹)₆(dmf)₂][PF₆]₂·2dmf and [Cu₄(L¹)₆(MeOH)₂][PF₆]₂·MeOH (Figs. 2–4) are centrosymmetric, so the asymmetric unit contains one half of the complex dication and one independent solvent molecule (dmf or MeOH, respectively); [Cu₄(L²)₄(dmf)₄][PF₆]₄·6dmf (Fig. 5) has no imposed symmetry, so each asymmetric unit contains an entire complex unit and six independent molecules of dmf.

CCDC reference number 186/1268.

See <http://www.rsc.org/suppdata/dt/1999/339/> for crystallographic files in .cif format.

Magnetic measurements

Magnetic susceptibilities of $[\text{Cu}_4(\text{L}^1)_6(\text{dmf})_2][\text{PF}_6]_2$ and $[\text{Cu}_4(\text{L}^2)_4(\text{dmf})_4][\text{PF}_6]_4$ were measured using a Mètronique Ingènierie MS-03 SQUID magnetometer in the temperature range 1.2–250 K. Both complexes possess an $S = 0$ ground state; the non-zero value of χT at low temperature is due to the temperature independent paramagnetism (TIP).

Magnetic data were interpreted by using the exchange spin Hamiltonians in the forms (1) and (2) for $[\text{Cu}_4(\text{L}^1)_6(\text{dmf})_2][\text{PF}_6]_2$

$$H_1 = J(S_1S_2 + S_{1a}S_{2a}) + J'(S_{1a}S_2 + S_{2a}S_1) \quad (1)$$

$$H_2 = J(S_1S_3 + S_1S_4 + S_2S_3 + S_2S_4) = J[(S_1 + S_2)(S_3 + S_4)] = J \cdot S_A S_B \quad (2)$$

and $[\text{Cu}_4(\text{L}^2)_4(\text{dmf})_4][\text{PF}_6]_4$, respectively. The eigenvalues for H_1 were computed with the CLUMAG program¹⁶ while those for H_2 were computed in the dimer scheme defining $S_A = (S_1 + S_2)$, $S_B = (S_3 + S_4)$ and $S_T = S_A + S_B$. In both cases the computed energies were used in the Van Vleck equation. The magnetic susceptibility data for both complexes were fitted by the theoretical equations by means of an iterative least-squares minimisation routine, and the results of these fits are indicated by the solid lines in Fig. 6.¹⁷ In both cases a contribution from a paramagnetic impurity (ρ) was included in the calculated susceptibility.

EPR spectroscopic measurements

The EPR spectra on powdered solids were recorded at *ca.* 9.5, 24.0 and 34.0 GHz using a Bruker ESP300-E spectrometer between 295 and 4.2 K. Spectra of solutions in dmf were also recorded at 110 K using the same instrumentation. The 90 GHz spectra, in the temperature range 100 to 10 K, were recorded on an induction mode spectrometer designed and developed at the University of St Andrews.¹⁸ This spectrometer used an 8T Oxford Instruments superconducting magnet. The source was a frequency doubled Gunn diode, phase locked to an EIP frequency counter. The EPR spectrum simulations were performed on a Digital 200/4/233 Alpha Workstation using programs described previously.¹⁹

Results and discussion

Complexes of HL¹

Compound HL¹ is a simple bidentate chelating ligand which also has the capacity, *via* deprotonation of the pyrazole NH group, to act as a dinucleating bridging ligand. We have recently observed both co-ordination modes in complexes with Fe^{III}, and have seen how deprotonation and consequent bridging behaviour can afford high nuclearity complexes.²⁰ Recently oligomeric complexes of L¹ with Cu^I and Ag^I have also been reported with the pyrazolate groups bridging.²¹ This prompted us to investigate the co-ordination behaviour of HL¹ with other transition metal cations.

Reaction of HL¹ with zinc(II) or nickel(II) salts affords the simple tris-chelates $[\text{M}(\text{HL}^1)_3]^{2+}$, here isolated as their hexafluorophosphate salts; this behaviour is in accord with that of various related pyridyl/pyrazole bidentate chelating ligands.²² The crystal structure of the complex cation $[\text{Zn}(\text{HL}^1)_3][\text{PF}_6]_2 \cdot \text{H}_2\text{O}$ is in Fig. 1; it is a simple mononuclear tris-chelate. Significant bond lengths and angles are collected in Table 2. The asymmetric bidentate ligands are arranged to give the sterically more favourable *mer* configuration in the pseudo-octahedral complex. One of the pyrazolyl NH groups [N(110)] is involved in a hydrogen bonding interaction to a water molecule, with the non-bonded O(1) \cdots N(110) separation being 2.784 Å.

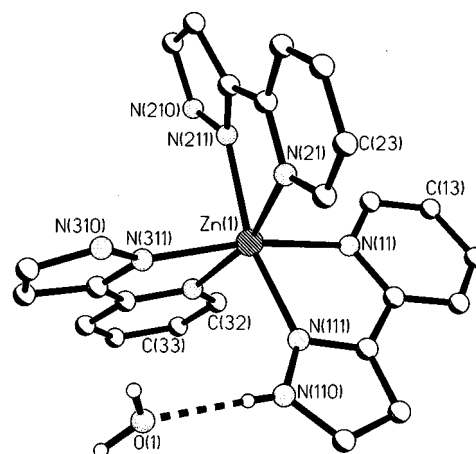


Fig. 1 Structure of the complex cation of $[\text{Zn}(\text{HL}^1)_3][\text{PF}_6]_2 \cdot \text{H}_2\text{O}$.

The nickel(II) complex $[\text{Ni}(\text{HL}^1)_3][\text{PF}_6]_2$ is isomorphous and isostructural with the zinc(II) complex; its bond lengths and angles are in Table 3. The electronic spectrum shows weak d–d transitions at 530 and 820 nm ($\epsilon = 54$ and $34 \text{ dm}^3 \text{ mol}^{-1} \text{ cm}^{-1}$ respectively) in CH_2Cl_2 whose position and intensity are entirely consistent with the complex having essentially octahedral geometry; for comparison, the two lower-energy d–d transitions of $[\text{Ni}(\text{bipy})_3]^{2+}$ are at 520 and 790 nm. The highest-energy d–d transition of $[\text{Ni}(\text{HL}^1)_3][\text{PF}_6]_2$ is hidden by the very strong ligand-centred transition at 286 nm. Thus, with metal ions that either have a stereoelectronic preference for octahedral geometry (*e.g.* Ni^{II}), or which have no particular aversion to it (*e.g.* Zn^{II}), HL¹ behaves as a simple bidentate chelating ligand and remains protonated.

Since Cu^{II} has a marked stereoelectronic preference for elongated tetragonal geometries, we thought it unlikely that the same type of complex would form between HL¹ and Cu^{II}. Reaction of HL¹ with $\text{Cu}(\text{O}_2\text{CCH}_3)_2 \cdot 2\text{H}_2\text{O}$ (3:2) in methanol at room temperature afforded a clear deep green solution from which a blue-green solid precipitated on addition of NH_4PF_6 ; this was crystallised from dmf–ether. FAB Mass spectrometry showed the presence of numerous peaks corresponding to polynuclear species [up to $\text{Cu}_4(\text{L}^1)_6$] and the elemental analysis was consistent with the empirical formula $[\text{Cu}_2(\text{L}^1)_3(\text{dmf})][\text{PF}_6]$. This product was formed using other ligand:metal stoichiometries, but the yield was subsequently optimised by using the required 3:2 ratio. The crystal structure (Fig. 2, Table 4) shows that the complex is in fact $[\text{Cu}_4(\text{L}^1)_6(\text{dmf})_2][\text{PF}_6]_2 \cdot 2\text{dmf}$. There are two approximately planar $\text{Cu}_2(\mu\text{-L}^1)_2$ units, related by an inversion centre, in which each $[\text{L}^1]^-$ acts as a terdentate bridge linking the two metal centres; these units are stacked parallel and face-to-face (interplane separation 3.2–3.5 Å), with additional deprotonated ligands $[\text{L}^1]^-$ perpendicular to the two $\text{Cu}_2(\mu\text{-L}^1)_2$ planes forming linking ‘cross-pieces’ between the $\text{Cu}_2(\mu\text{-L}^1)_2$ units. Two of the metals [Cu(1) and Cu(1A)] have additional dmf ligands attached, and therefore have a square-pyramidal N_4O environment in which the O ligands (dmf) are axial; Cu(2) and Cu(2A) have square-pyramidal N_5 environments in which one of the pyrazole donor atoms is in the axial position. In every case the axial ligand is significantly further from the metal [Cu(1)–O(51), 2.339(2); Cu(2)–N(411A), 2.198(2) Å] than the four equatorial ligands (lengths in the range 1.97–2.07 Å), in keeping with the requirements of the Jahn–Teller effect.

A significant feature of this complex is the ease with which the axial dmf ligands are lost. An IR spectrum of the crystalline material shows strong peaks at 1670 and 1654 cm^{-1} , which we assign to the carbonyl stretching vibrations of non-coordinated (lattice) and co-ordinated dmf respectively, in agreement with the crystal structure. For free dmf, ν_{CO} can vary from about 1655 to 1695 cm^{-1} depending on the extent of hydrogen

Table 1 Crystallographic data for the five crystal structures

	[Zn(HL ¹) ₃][PF ₆] ₂ ·H ₂ O	[Ni(HL ¹) ₃][PF ₆] ₂ ·H ₂ O	[Cu ₄ (L ¹) ₆ (dmf) ₂][PF ₆] ₂ ·2dmf	[Cu ₄ (L ¹) ₆ (MeOH) ₂][PF ₆] ₂ ·2MeOH	[Cu ₄ (L ²) ₄ (dmf) ₄][PF ₆] ₄ ·6dmf
Formula	C ₂₄ H ₂₃ F ₁₂ N ₉ OP ₂ Zn	C ₂₄ H ₂₃ F ₁₂ N ₉ NiOP ₂	C ₆₀ H ₆₄ Cu ₄ F ₁₂ N ₂₂ O ₄ P ₂	C ₅₂ H ₅₂ Cu ₄ F ₁₂ N ₁₈ O ₄ P ₂	C ₈₂ H ₁₀₆ Cu ₄ F ₂₄ N ₂₆ O ₁₀
<i>M</i>	808.82	802.16	1701.43	1537.22	2449.97
System, space group	Monoclinic, <i>P2₁/n</i>	Monoclinic, <i>P2₁/n</i>	Triclinic, <i>P$\bar{1}$</i>	Triclinic, <i>P$\bar{1}$</i>	Monoclinic, <i>P2₁/n</i>
<i>a</i> /Å	11.5877(14)	11.531(3)	10.410(2)	10.888(2)	19.567(2)
<i>b</i> /Å	12.651(2)	12.642(3)	13.282(3)	12.739(2)	26.313(3)
<i>c</i> /Å	21.630(4)	21.607(5)	14.170(2)	13.050(2)	20.033(3)
<i>a</i> °			85.254(10)	116.745(8)	
<i>β</i> °	96.208(13)	96.26(2)	70.087(12)	101.313(11)	91.441(10)
<i>γ</i> °			68.15(2)	102.246(13)	
<i>U</i> /Å ³	3152.3(8)	3130.8(13)	1707.5(6)	1488.8(4)	10311(3)
<i>Z</i>	4	4	1	1	4
<i>D_c</i> /g cm ⁻³	1.704	1.698	1.655	1.712	1.578
<i>μ</i> /mm ⁻¹	0.989	0.831	1.373	1.560	0.987
<i>F</i> (000)	1624	1608	864	776	5008
Crystal size/mm	0.5 × 0.4 × 0.1	0.2 × 0.1 × 0.1	0.5 × 0.4 × 0.1	0.3 × 0.2 × 0.1	0.7 × 0.15 × 0.1
Reflections collected: total, independent, <i>R</i> _{int}	14695, 5537, 0.0353	19307, 7100, 0.0627	8183, 5820, 0.0227	15396, 6727, 0.0343	63226, 23223, 0.0793
2 θ limits for data°	5–50	4–55	4–50	4–55	3–55
Data, restraints, parameters	5532, 1, 469	7100, 0, 442	5820, 0, 473	6727, 0, 480	23223, 0, 1445
Final <i>R</i> 1, <i>wR</i> 2 ^{<i>a,b</i>}	0.0603, 0.1699	0.0615, 0.1646	0.0360, 0.1056	0.0380, 0.0943	0.0792, 0.2000
Weighting factors ^{<i>a</i>}	0.0783, 9.7755	0.0685, 3.2831	0.0686, 3.0096	0.0492, 0	0.0641, 21.66
Largest peak, hole/e Å ⁻³	+1.405, -0.689	+0.990, -0.509	+0.703, -0.506	+0.725, -0.903	+1.005, -0.757

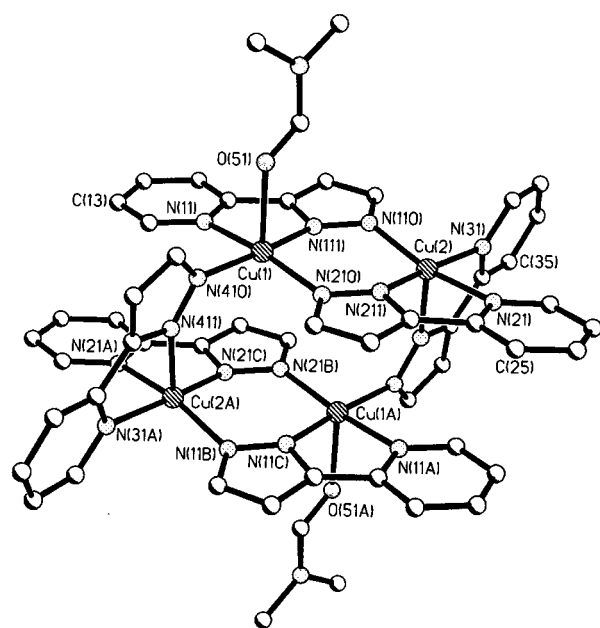
^{*a*} Structure was refined on F_o^2 using all data; the value of *R*1 is given for comparison with older refinements based on F_o with a typical threshold of $F \geq 4\sigma(F)$. ^{*b*} $wR2 = [\sum w(F_o^2 - F_c^2)^2 / \sum w(F_o^2)^2]^{1/2}$ where $w^{-1} = \sigma^2(F_o^2) + (aP)^2 + bP$ and $P = [\max(F_o^2, 0) + 2F_c^2]/3$.

Table 2 Selected bond lengths (Å) and angles (°) for $[\text{Zn}(\text{L}^1)_3][\text{PF}_6]_2 \cdot \text{H}_2\text{O}$

Zn(1)–N(111)	2.129(4)	Zn(1)–N(211)	2.160(4)
Zn(1)–N(311)	2.141(4)	Zn(1)–N(31)	2.192(4)
Zn(1)–N(11)	2.149(4)	Zn(1)–N(21)	2.201(4)
N(111)–Zn(1)–N(311)	97.00(14)	N(11)–Zn(1)–N(31)	96.9(2)
N(111)–Zn(1)–N(11)	76.50(14)	N(211)–Zn(1)–N(31)	95.73(14)
N(311)–Zn(1)–N(11)	169.5(2)	N(111)–Zn(1)–N(21)	91.38(14)
N(111)–Zn(1)–N(211)	163.72(14)	N(311)–Zn(1)–N(21)	92.08(14)
N(311)–Zn(1)–N(211)	92.76(14)	N(11)–Zn(1)–N(21)	96.28(14)
N(11)–Zn(1)–N(211)	95.50(14)	N(211)–Zn(1)–N(21)	75.22(14)
N(111)–Zn(1)–N(31)	99.27(14)	N(31)–Zn(1)–N(21)	164.71(14)
N(311)–Zn(1)–N(31)	75.8(2)		

Table 3 Selected bond lengths (Å) and angles (°) for $[\text{Ni}(\text{HL}^1)_3][\text{PF}_6]_2 \cdot \text{H}_2\text{O}$

Ni(1)–N(31)	2.056(4)	Ni(1)–N(41)	2.101(4)
Ni(1)–N(51)	2.074(4)	Ni(1)–N(61)	2.127(4)
Ni(1)–N(11)	2.080(4)	Ni(1)–N(21)	2.128(4)
N(31)–Ni(1)–N(51)	95.66(14)	N(11)–Ni(1)–N(61)	94.96(14)
N(31)–Ni(1)–N(11)	167.53(14)	N(41)–Ni(1)–N(61)	95.67(14)
N(51)–Ni(1)–N(11)	91.82(14)	N(31)–Ni(1)–N(21)	92.15(14)
N(31)–Ni(1)–N(41)	78.43(14)	N(51)–Ni(1)–N(21)	92.50(14)
N(51)–Ni(1)–N(41)	170.72(14)	N(11)–Ni(1)–N(21)	77.54(14)
N(11)–Ni(1)–N(41)	95.28(14)	N(41)–Ni(1)–N(21)	94.85(14)
N(31)–Ni(1)–N(61)	96.36(14)	N(61)–Ni(1)–N(21)	167.60(14)
N(51)–Ni(1)–N(61)	77.8(2)		

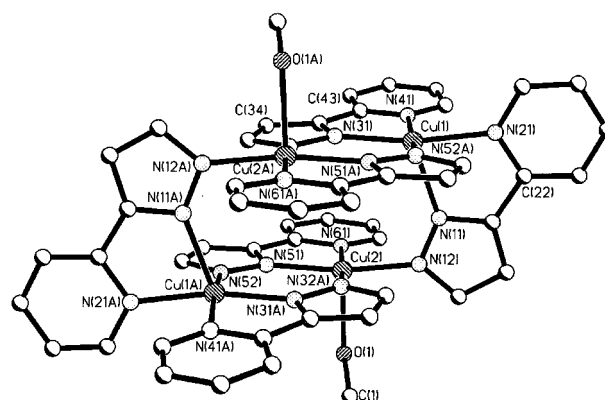
**Fig. 2** Structure of the complex cation of $[\text{Cu}_4(\text{L}^1)_6(\text{dmf})_2][\text{PF}_6]_2 \cdot 2\text{dmf}$.

bonding to the carbonyl group;²³ the band generally moves to lower energy on co-ordination to a metal ion.²⁴ On grinding the crystals and oven drying at about 70 °C, IR spectra taken at regular intervals showed that the 1670 cm^{-1} band disappears first, followed more slowly by the 1654 cm^{-1} band. After 24 h oven drying there was no trace of any lattice or co-ordinated dmf, and the elemental analysis of the dried material was consistent with this. The fact that crystallisation of this from dmf-ether afforded again crystals of $[\text{Cu}_4(\text{L}^1)_6(\text{dmf})_2][\text{PF}_6]_2 \cdot 2\text{dmf}$ confirms that loss of axial solvent molecules does not result in decomposition of the cluster core. The sample used for magnetic susceptibility measurements was dried in this way.

Crystallisation of the above complex from methanol also resulted in a crystalline material, whose FAB mass spectrum was essentially identical to that of the dmf solvate and whose

Table 4 Selected bond lengths (Å) and angles (°) for $[\text{Cu}_4(\text{L}^1)_6(\text{dmf})_2][\text{PF}_6]_2 \cdot 2\text{dmf}$

Cu(1)–N(410)	1.977(2)	Cu(2)–N(211)	1.968(2)
Cu(1)–N(210)	1.980(2)	Cu(2)–N(110)	1.996(2)
Cu(1)–N(111)	1.982(2)	Cu(2)–N(31)	2.047(2)
Cu(1)–N(11)	2.064(2)	Cu(2)–N(21)	2.073(2)
Cu(1)–O(51)	2.339(2)	Cu(2)–N(411A)	2.198(2)
N(410)–Cu(1)–N(210)	91.57(9)	N(211)–Cu(2)–N(110)	96.60(9)
N(410)–Cu(1)–N(111)	170.61(9)	N(211)–Cu(2)–N(31)	171.35(9)
N(210)–Cu(1)–N(111)	96.64(9)	N(110)–Cu(2)–N(31)	90.31(9)
N(410)–Cu(1)–N(11)	90.51(9)	N(211)–Cu(2)–N(21)	80.72(9)
N(210)–Cu(1)–N(11)	168.85(9)	N(110)–Cu(2)–N(21)	165.66(9)
N(111)–Cu(1)–N(11)	80.57(9)	N(31)–Cu(2)–N(21)	91.31(9)
N(410)–Cu(1)–O(51)	89.00(9)	N(211)–Cu(2)–N(411A)	105.84(9)
N(210)–Cu(1)–O(51)	98.09(9)	N(110)–Cu(2)–N(411A)	96.37(9)
N(111)–Cu(1)–O(51)	94.35(9)	N(31)–Cu(2)–N(411A)	78.44(9)
N(11)–Cu(1)–O(51)	92.90(9)	N(21)–Cu(2)–N(411A)	97.92(9)

**Fig. 3** Structure of the complex cation of $[\text{Cu}_4(\text{L}^1)_6(\text{MeOH})_2][\text{PF}_6]_2 \cdot 2\text{MeOH}$.

elemental analysis also suggested a 3:2 ligand:metal ratio. Crystal structure analysis (Fig. 3, Table 5) showed this complex to be $[\text{Cu}_4(\text{L}^1)_6(\text{MeOH})_2][\text{PF}_6]_2 \cdot 2\text{MeOH}$, essentially identical to $[\text{Cu}_4(\text{L}^1)_6(\text{dmf})_2][\text{PF}_6]_2 \cdot 2\text{dmf}$ but with the dmf molecules (both co-ordinated and free in the lattice) replaced by methanol molecules. The grid-like core of the structure is therefore sufficiently robust not to be affected by changing the relatively labile monodentate solvent ligands. The $\text{Cu} \cdots \text{Cu}$ separations in the methanol solvate (3.939 and 3.984 Å) are similar to those observed in the dmf solvate above (3.963 and 4.080 Å), so the $\{\text{Cu}_4(\text{L}^1)_6\}^{2+}$ core is not substantially affected by the change of co-ordinating solvent. Fig. 4(a) emphasises the grid-like structure of the molecules. We assume that the axial solvent molecules are also labile in this complex, but did not investigate this further.

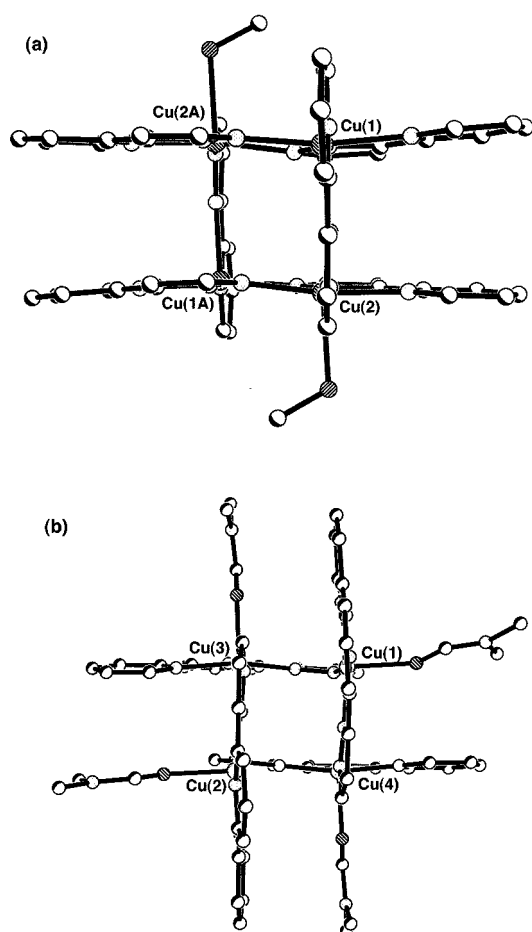
The dinuclear $\text{Cu}_2(\mu\text{-L}^1)_2$ units of these complexes are reminiscent of the dinuclear complexes of the bridging ligand 3,5-bis(2-pyridyl)pyrazole, which forms planar $[\text{M}_2\text{L}_2]^{n+}$ complexes having two deprotonated pyrazolate bridges with various metal ions.^{10e} It is clear from comparison of the structures of the copper(II) complexes of L^1 with those of the mononuclear nickel(II) and zinc(II) analogues that the assembly of the grid-like architectures is driven principally by the stereoelectronic preference of the copper(II) ions for elongated tetragonal geometry: to satisfy this requirement necessitates deprotonation of the pyrazole rings and bridging behaviour of the ligand. We note that the particular stereoelectronic preferences of the copper(II) ion have also been exploited recently in directing the assembly of double helicates in which the two ligand strands are different.²⁵

Complexes of HL^2

We described the preparation of HL^2 recently, but used it as a

Table 5 Selected bond lengths (Å) and angles (°) for $[\text{Cu}_4(\text{L}^1)_6(\text{MeOH})_2][\text{PF}_6]_2 \cdot 2\text{MeOH}$

Cu(1)–N(31)	1.983(2)	Cu(2)–N(51)	1.982(2)
Cu(1)–N(52A)	1.999(2)	Cu(2)–N(32A)	1.982(2)
Cu(1)–N(21)	2.072(2)	Cu(2)–N(12)	1.991(2)
Cu(1)–N(41)	2.076(2)	Cu(2)–N(61)	2.072(2)
Cu(1)–N(11)	2.196(2)	Cu(2)–O(1)	2.349(2)
N(31)–Cu(1)–N(52A)	97.23(9)	N(51)–Cu(2)–N(32A)	97.34(9)
N(31)–Cu(1)–N(21)	168.30(9)	N(51)–Cu(2)–N(12)	168.89(9)
N(52A)–Cu(1)–N(21)	89.67(9)	N(32A)–Cu(2)–N(12)	90.39(9)
N(31)–Cu(1)–N(41)	80.49(9)	N(51)–Cu(2)–N(61)	80.60(9)
N(52A)–Cu(1)–N(41)	170.12(9)	N(32A)–Cu(2)–N(61)	172.00(9)
N(21)–Cu(1)–N(41)	91.11(9)	N(12)–Cu(2)–N(61)	90.65(9)
N(31)–Cu(1)–N(11)	110.40(9)	N(51)–Cu(2)–O(1)	92.80(9)
N(52A)–Cu(1)–N(11)	96.73(9)	N(32A)–Cu(2)–O(1)	100.28(9)
N(21)–Cu(1)–N(11)	77.96(8)	N(12)–Cu(2)–O(1)	93.66(9)
N(41)–Cu(1)–N(11)	93.06(8)	N(61)–Cu(2)–O(1)	87.57(9)

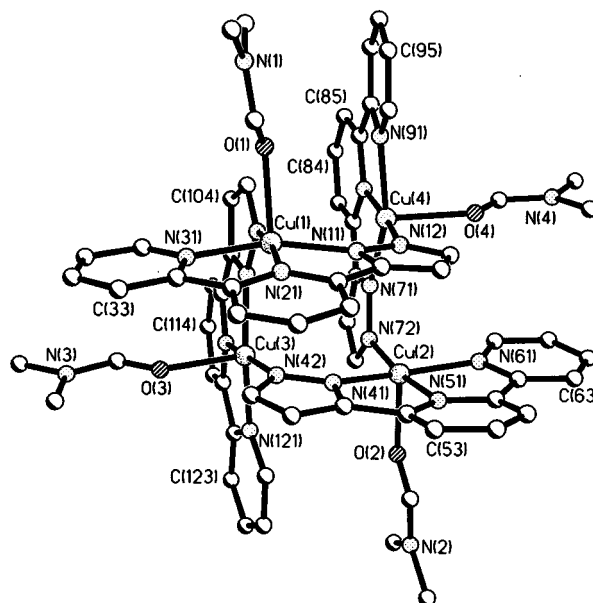
**Fig. 4** Edge-on views of the tetranuclear complex cations, emphasizing the grid-like structure: (a) $[\text{Cu}_4(\text{L}^1)_6(\text{MeOH})_2]^{2+}$; (b) $[\text{Cu}_4(\text{L}^2)_4(\text{dmf})_4]^{4+}$.

precursor to a new hexadentate ligand and did not investigate its co-ordination properties.¹³ By analogy with HL^1 it seemed likely that HL^2 could behave as a simple terdentate chelating ligand to just one metal centre, or alternatively could act as a dinucleating bridging ligand *via* deprotonation of the pyrazole.

Reaction of HL^2 with nickel(II) acetate or zinc(II) acetate in methanol, followed by treatment of the solution with NH_4PF_6 , afforded complexes whose mass spectra and elemental analyses indicated that they were mononuclear complexes of formulation $[\text{M}(\text{HL}^2)_2][\text{PF}_6]_2$. We could not get X-ray quality crystals of them but they are likely to be unremarkable mononuclear octahedral complexes, and will not be discussed further here. In contrast, reaction with copper(II) acetate followed by precipitation of the complex as its hexafluorophosphate salt afforded a

Table 6 Selected bond lengths (Å) and angles (°) for $[\text{Cu}_4(\text{L}^2)_4(\text{dmf})_4][\text{PF}_6]_4 \cdot 6\text{dmf}$

Cu(1)–N(102)	1.948(5)	Cu(3)–N(42)	1.952(5)
Cu(1)–N(21)	1.956(5)	Cu(3)–N(111)	1.955(5)
Cu(1)–N(11)	2.002(5)	Cu(3)–N(101)	2.009(5)
Cu(1)–N(31)	2.049(5)	Cu(3)–N(121)	2.056(5)
Cu(1)–O(1)	2.243(4)	Cu(3)–O(3)	2.230(4)
Cu(2)–N(72)	1.952(4)	Cu(4)–N(12)	1.949(5)
Cu(2)–N(51)	1.953(5)	Cu(4)–N(81)	1.961(5)
Cu(2)–N(41)	2.012(5)	Cu(4)–N(71)	2.011(4)
Cu(2)–N(61)	2.049(5)	Cu(4)–N(91)	2.041(4)
Cu(2)–O(2)	2.270(4)	Cu(4)–O(4)	2.226(4)
N(102)–Cu(1)–N(21)	168.4(2)	N(42)–Cu(3)–N(111)	170.2(2)
N(102)–Cu(1)–N(11)	102.5(2)	N(42)–Cu(3)–N(101)	105.2(2)
N(21)–Cu(1)–N(11)	79.7(2)	N(111)–Cu(3)–N(101)	79.4(2)
N(102)–Cu(1)–N(31)	96.0(2)	N(42)–Cu(3)–N(121)	94.3(2)
N(21)–Cu(1)–N(31)	79.7(2)	N(111)–Cu(3)–N(121)	79.4(2)
N(11)–Cu(1)–N(31)	157.6(2)	N(101)–Cu(3)–N(121)	156.4(2)
N(102)–Cu(1)–O(1)	92.1(2)	N(42)–Cu(3)–O(3)	89.6(2)
N(21)–Cu(1)–O(1)	98.8(2)	N(111)–Cu(3)–O(3)	98.1(2)
N(11)–Cu(1)–O(1)	99.1(2)	N(101)–Cu(3)–O(3)	100.5(2)
N(31)–Cu(1)–O(1)	92.7(2)	N(121)–Cu(3)–O(3)	92.8(2)
N(72)–Cu(2)–N(51)	171.6(2)	N(12)–Cu(4)–N(81)	171.9(2)
N(72)–Cu(2)–N(41)	103.8(2)	N(12)–Cu(4)–N(71)	103.6(2)
N(51)–Cu(2)–N(41)	79.4(2)	N(81)–Cu(4)–N(71)	79.4(2)
N(72)–Cu(2)–N(61)	95.6(2)	N(12)–Cu(4)–N(91)	96.5(2)
N(51)–Cu(2)–N(61)	79.7(2)	N(81)–Cu(4)–N(91)	79.0(2)
N(41)–Cu(2)–N(61)	156.8(2)	N(71)–Cu(4)–N(91)	156.1(2)
N(72)–Cu(2)–O(2)	91.1(2)	N(12)–Cu(4)–O(4)	88.7(2)
N(51)–Cu(2)–O(2)	96.1(2)	N(81)–Cu(4)–O(4)	98.3(2)
N(41)–Cu(2)–O(2)	100.2(2)	N(71)–Cu(4)–O(4)	100.4(2)
N(61)–Cu(2)–O(2)	92.0(2)	N(91)–Cu(4)–O(4)	92.8(2)

**Fig. 5** Structure of the complex cation of $[\text{Cu}_4(\text{L}^2)_4(\text{dmf})_4][\text{PF}_6]_4 \cdot 6\text{dmf}$.

blue-green solid which was crystallised from dmf –ether to give dark green X-ray quality crystals in high yield. Electrospray mass spectrometry indicated formation of a tetranuclear complex in solution, with the peak at the highest m/z value corresponding to $\{\text{Cu}_4(\text{L}^2)_4(\text{PF}_6)_2\}^{2+}$. The elemental analysis indicated the empirical formula $[\text{Cu}(\text{L}^2)][\text{PF}_6]$, *i.e.* a 1 : 1 metal : ligand ratio. The crystal structure (Fig. 5, Table 6) revealed the complex to be the tetramer $[\text{Cu}_4(\text{L}^2)_4(\text{dmf})_4][\text{PF}_6]_4 \cdot 6\text{dmf}$. This has many structural similarities to $[\text{Cu}_4(\text{L}^1)_6(\text{solv})_2][\text{PF}_6]_2$ ($\text{solv} = \text{dmf}$ or MeOH) (above). The overall structure is that of a 2×2 grid, with two pairs of parallel, stacked $[\text{L}^2]^-$ ligands mutually perpendicular to each other. The stacking distances between overlapping aromatic ligand fragments again are in the range 3.2–3.5 Å. Each metal ion is co-ordinated by the ter-

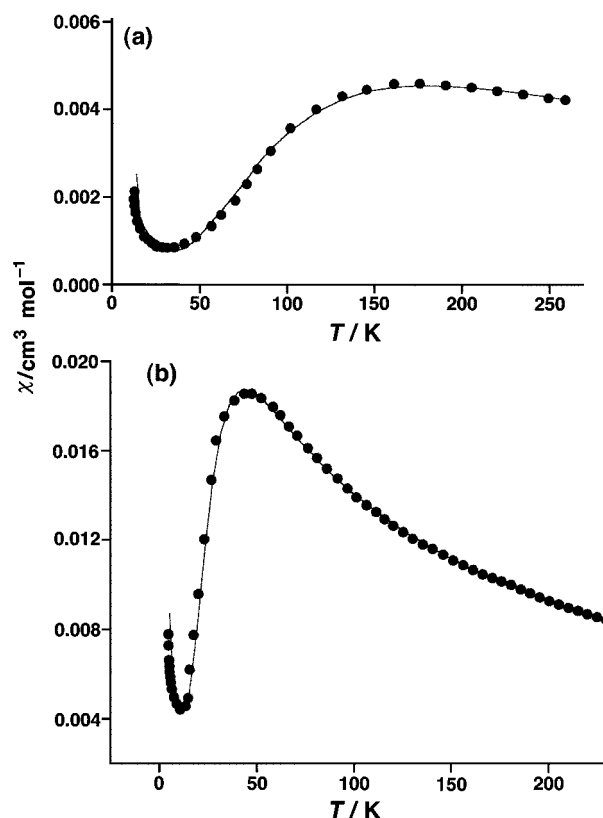


Fig. 6 Plots of χ vs. T for (a) $[\text{Cu}_4(\text{L}^1)_6][\text{PF}_6]_2$ and (b) $[\text{Cu}_4(\text{L}^2)_4][\text{PF}_6]_4$. The circles are measured data; the line is the calculated fit based on the parameters given in the text.

dentate pocket of one deprotonated ligand $[\text{L}^2]^-$, one pyrazole donor atom which is acting as a bridge to a ligand attached to another metal ion, and a dmf ligand. The result is an elongated N_4O square-pyramidal geometry with the dmf ligand in the axial position; the axial bond lengths lie in the range 2.23–2.27 Å, in contrast to the equatorial ones which lie in the range 1.95–2.06 Å. The four metal ions are crystallographically independent but chemically very similar, and the complex has approximate S_4 symmetry *{cf.}* the S_2 axis of $[\text{Cu}_4(\text{L}^1)_6(\text{dmf})_2][\text{PF}_6]_2$ implied by its inversion centre}. Fig. 4(b) shows an edge-on view of the complex cation. The four copper(II) ions are not now coplanar, but form a butterfly-like arrangement with the metal ions around the Cu_4 ring alternately above and below their mean plane. As with the copper(II) complexes of L^1 , it is clear that the formation of this structure is driven by the stereoelectronic preference of copper(II) ions for an elongated tetragonal geometry.

Again the dmf ligands are labile; the initially crystallised material has a broad, strong carbonyl signal at 1656 cm^{-1} with a high-energy shoulder just discernible, which we assign to co-ordinated dmf and free (lattice) dmf molecules respectively, in agreement with the crystal structure. On heating these completely disappear, and the elemental analysis of the resulting material is consistent with the formulation $[\text{Cu}_4(\text{L}^2)_4][\text{PF}_6]_4$; this is the material that was used for magnetic studies (below).

Magnetic susceptibility studies

The complexes $[\text{Cu}_4(\text{L}^1)_6][\text{PF}_6]_2$ and $[\text{Cu}_4(\text{L}^2)_4][\text{PF}_6]_4$, in which the axial solvent ligands have been removed, were subjected to magnetic susceptibility measurements in the temperature range 1.2–250 K; plots of χ vs. T are given in Fig. 6. The room temperature value of χ for $[\text{Cu}_4(\text{L}^1)_6][\text{PF}_6]_2$ is much smaller than expected for uncoupled spins, suggesting dominant antiferromagnetic coupling within the cluster. This is confirmed by the broad maximum in the susceptibility observed at *ca.* 170 K

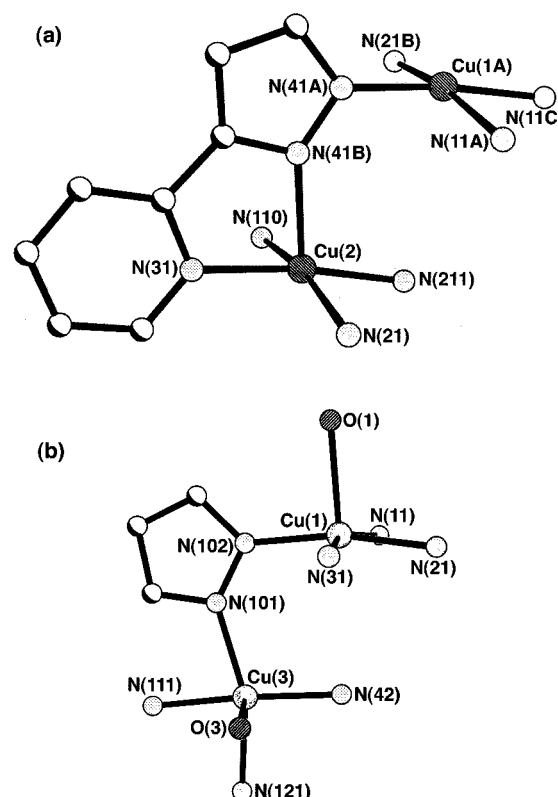


Fig. 7 Excerpts from the crystal structures of (a) $[\text{Cu}_4(\text{L}^1)_6(\text{dmf})_2][\text{PF}_6]_2$ and (b) $[\text{Cu}_4(\text{L}^2)_4(\text{dmf})_4][\text{PF}_6]_4$, emphasising the geometry of the bridging groups.

[Fig. 6(a)]. At low temperature the compound is essentially diamagnetic. The increase in χ below 20 K is presumably due to some paramagnetic impurity. A maximum is observed also in the susceptibility of $[\text{Cu}_4(\text{L}^2)_4][\text{PF}_6]_4$ at *ca.* 50 K, again suggesting a dominant antiferromagnetic coupling, albeit weaker than in $[\text{Cu}_4(\text{L}^1)_6][\text{PF}_6]_2$.

The best fit values derived from the susceptibility data for $[\text{Cu}_4(\text{L}^2)_4][\text{PF}_6]_4$ are $g = 2.35$, $\rho = 6.5\%$, $J = 63.5\text{ cm}^{-1}$.[†] Although the complex has no crystallographically imposed symmetry and all four $\text{Cu} \cdots \text{Cu}$ couplings could therefore be slightly different, the susceptibility data can be satisfactorily accounted for by a single antiferromagnetic coupling constant of 63.5 cm^{-1} along each edge of the Cu_4 ring. The complex accordingly has an $S = 0$ ground state. The (approximate) S_4 symmetry of the complex means that the magnetic $d(x^2 - y^2)$ orbital on each metal is effectively at 90° to each of its neighbours, although each pyrazolate bridge does span two magnetic orbitals. This is illustrated in Fig. 7(b). At Cu(1) the plane of the magnetic orbital is defined by the equatorial donor atoms N(102), N(11), N(21) and N(31); *i.e.* it is being viewed 'edge-on' in the Figure. At Cu(3) the four equatorial donor atoms are N(101), N(42), N(121) and N(111), *i.e.* in the plane of the paper. Thus the two magnetic orbitals are *spatially* orthogonal to one another,

[†] We note that the g values derived from the magnetic susceptibility data do not agree well with those derived from EPR spectra, which are far more reliable. This is quite common and arises because a g value derived from magnetic susceptibility data acts as a sink for all of the systematic errors in the curve fitting, and therefore has little significance. For $[\text{Cu}_4(\text{L}^1)_6][\text{PF}_6]_2$ the strong correlation between J and J' inevitably causes problems with the fitting. In $[\text{Cu}_4(\text{L}^2)_4][\text{PF}_6]_4$ we have assumed that all four coupling pathways are equivalent, despite the fact that they are crystallographically slightly inequivalent. In addition it is entirely possible that the co-ordinatively unsaturated copper(II) centres could pick up axial water ligands from the air, at the sites vacated by the dmf ligands after drying: this would result in slight errors in the molecular weights used and in the diamagnetic correction, both of which would affect the derived g values (but not the J values).

although they are of the same symmetry species and can therefore mix, and they are both linked by atoms N(101) and N(102) of the pyrazolate bridge. The result here is antiferromagnetic exchange, although it is rather weak. This is in agreement with the magnetic behaviour of a related tetranuclear copper(II) complex which has the same symmetry properties, *viz.* a diazene bridge linking mutually perpendicular magnetic orbitals in a tetranuclear complex of S_4 symmetry: the antiferromagnetic coupling constant in this case was even weaker, at 12.2 cm^{-1} .²⁶

Matters were slightly more complex in the fitting procedure of the susceptibility of $[\text{Cu}_4(\text{L}^1)_6(\text{dmf})_2][\text{PF}_6]_2$ because the two parameters J and J' which are needed are strongly correlated. The observed maximum at *ca.* 170 K suggests that there is at least one antiferromagnetic exchange constant J of *ca.* 170 cm^{-1} , but no direct information is available on the second one. In fact sample calculations showed that acceptable fits can be obtained, either with two similar values for J and J' , or with $J > 170 \text{ cm}^{-1}$ and $J' < 170 \text{ cm}^{-1}$. The best fit values are $g = 2.23$, $\rho = 5.9\%$, $J = 172 \text{ cm}^{-1}$, $J' = 155 \text{ cm}^{-1}$.[†] We interpret these values as a lower limit for J and as an upper limit for J' , and assume that the larger value is associated with the double pyrazolate bridge. The fact that both interactions are antiferromagnetic means that $[\text{Cu}_4(\text{L}^1)_6][\text{PF}_6]_2$ also has an $S = 0$ ground state in which the four unpaired electrons will alternate in orientation around the Cu_4 ring. The stronger coupling ($J \geq 172 \text{ cm}^{-1}$) is within each doubly bridged $\{\text{Cu}_2(\text{L}^1)_2\}$ plane, *i.e.* between Cu(1) and Cu(2), and likewise between Cu(1A) and Cu(2A). It is to be expected that a strong antiferromagnetic coupling would occur in these cases as the magnetic $d(x^2 - y^2)$ orbitals are coplanar and overlap with the σ orbitals of the coplanar bridging pyrazolate fragments. This is a common type of structure^{9,10} and it is well understood how antiferromagnetism arises in such cases.⁹

The weaker antiferromagnetic coupling of $J' \leq 155 \text{ cm}^{-1}$ is between the singly bridged pair Cu(1) and Cu(2A), and likewise between Cu(2) and Cu(1A). The magnitude of this is less easy to understand because (i) there is only one bridging pyrazolate group, and (ii) it does not appear to interact with both magnetic orbitals on the two metal centres that it bridges. The relevant section of the crystal structure is shown in Fig. 7(a); whereas one of the pyrazolate donors [N(41A)] overlaps with the $d(x^2 - y^2)$ orbital of Cu(1A), the second [N(41B)] co-ordinates to Cu(2) along its z axis, orthogonal to the magnetic orbital. There are two possible answers to this problem. First, an additional coupling pathway exists *via* the pyridyl donor: the $d(x^2 - y^2)$ orbital on Cu(2) interacts with the pyridyl donor N(31) even though it does not interact with the pyrazolyl donor N(41B). Thus there is an additional Cu(1A)–pyrazolyl(N41A)–pyridyl(N31)–Cu(2) pathway which could provide a contribution to antiferromagnetic exchange. Secondly, the geometries about the copper centres are slightly distorted from regular square pyramidal. This provides a mechanism for some mixing of the $d(x^2 - y^2)$ and $d(z^2)$ orbitals, which are only orthogonal in high symmetries, such that the ‘axial’ pyrazolate donor N(41B) will interact with the unpaired electron on Cu(2) to some extent. However we emphasise that the derived value of J' is only an upper limit: because of the strong correlation between J and J' , the actual value could be considerably lower.

EPR spectroscopic studies

The EPR spectra of $[\text{Cu}_4(\text{L}^1)_6][\text{PF}_6]_2$ as a powder at room temperature consist mainly of a broad feature in the “ $g = 2$ ” region at X-, K- and Q-band frequencies (Fig. 8). On cooling to 100 K these spectra showed some resolution, particularly at the higher frequencies. At 100 K a weak half-field feature was found in the spectra at all three frequencies, which is most apparent in Fig. 8(a) (X-band). Further cooling at K-band, and also spectra below 100 K at W-band, resulted in an overall decrease in the spectrum intensity accompanied by a relatively more rapid

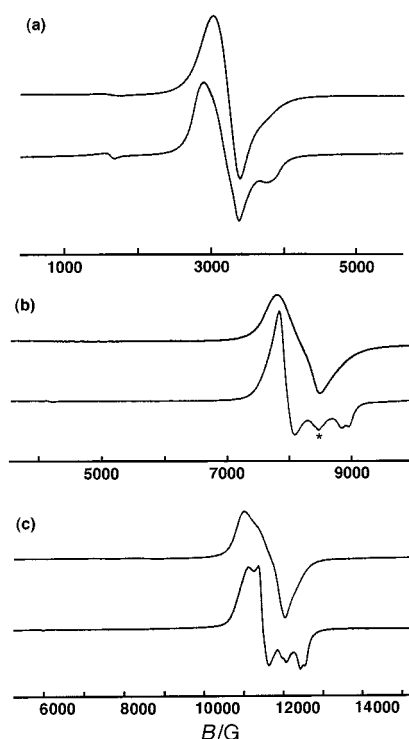


Fig. 8 Experimental spectra of a powder of $[\text{Cu}_4(\text{L}^1)_6(\text{dmf})_2][\text{PF}_6]_2$ at (a) X-band, (b) K-band and (c) Q-band. In each case the upper spectrum is at 295 K and the lower is at 100 K.

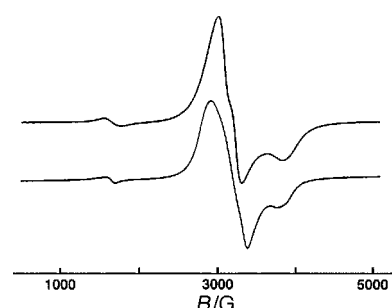


Fig. 9 Experimental (lower line) and simulated (upper line) EPR spectra of $[\text{Cu}_4(\text{L}^1)_6][\text{PF}_6]_2$ as a powder at X-band and 100 K.

decrease in the feature marked * in the K-band spectrum at 100 K [Fig. 8(b)]. The main features in the spectra at 100 K at all four frequencies were well simulated as a spin-triplet spectrum, using the same set of spin-Hamiltonian parameters [$g_x = 2.220$, $g_y = 2.060$, $g_z = 2.050$, $D = 0.050 \text{ cm}^{-1}$, $\lambda (=E/D) = 0.22$]; see Figs. 9 and 10 for two representative examples. The axis for g_z and the principal axis of the zero-field splitting (D_{zz}) are assumed to be coincident. We have been unable to simulate the feature marked *, which we therefore tentatively attribute to the expected quintet state (see below). The good simulations at four different frequencies indicates that the parameters for the spin-triplet state are reliable. In addition, the temperature variation of the intensity of the spin-triplet spectrum confirms that this is not the ground state, in agreement with the magnetic susceptibility results.

For $[\text{Cu}_4(\text{L}^2)_4][\text{PF}_6]_4$ the spectra at X-band are less well resolved than those for $[\text{Cu}_4(\text{L}^1)_6][\text{PF}_6]_2$. For this reason we concentrated on the spectra at both Q- and W-band (90 GHz). Representative spectra at both of these frequencies are in Figs. 11 and 12. These spectra are well simulated assuming that they arise from a spin-triplet state. At any given temperature the spin-Hamiltonian parameters required for the simulations at both frequencies are the same within experimental error (at 100 K, $g_{\parallel} = 2.033$, $g_{\perp} = 2.130$, $D = 0.017 \text{ cm}^{-1}$, $\lambda = 0$). However,

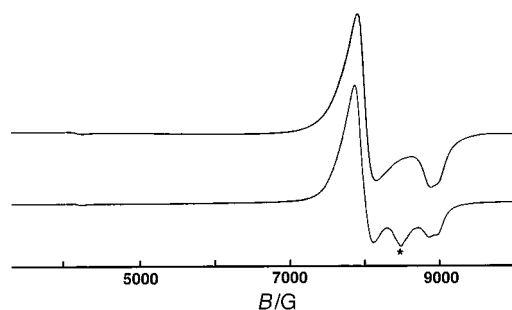


Fig. 10 Experimental (lower line) and simulated (upper line) EPR spectra of $[\text{Cu}_4(\text{L}^1)_6][\text{PF}_6]_2$ as a powder at K-band and 100 K.

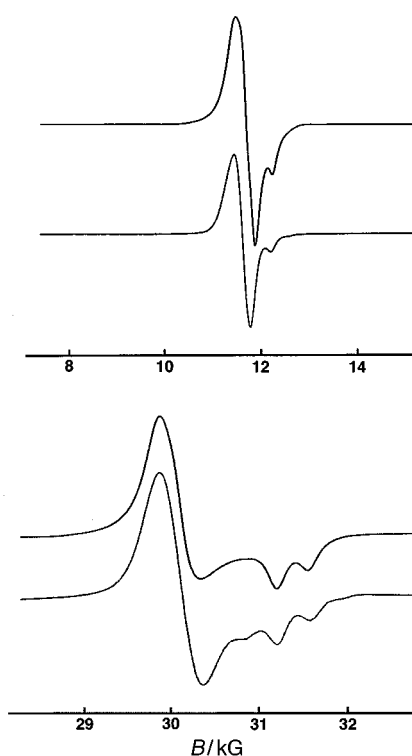


Fig. 11 Experimental (lower line) and simulated (upper line) EPR spectra of $[\text{Cu}_4(\text{L}^2)_4][\text{PF}_6]_4$ under the following conditions: (a) powder spectrum, Q-band, 100 K; (b) powder spectrum, W-band, 100 K.

there appears to be a small increase in D as the temperature decreases (0.017 cm^{-1} at 100 K to 0.030 cm^{-1} at 10 K). These spectra are axial, with the rather unusual situation that $g_{\parallel} < g_{\perp}$. It is noticeable that the g_{\parallel} value is very similar to that of the smallest g value of $[\text{Cu}_4(\text{L}^1)_6][\text{PF}_6]_2$, whereas the g_{\perp} value is approximately the average of the other two g values for $[\text{Cu}_4(\text{L}^1)_6][\text{PF}_6]_2$. This is understandable given the approximate S_4 symmetry of the complex. If the principal axes of Cu(1) are taken to be along the metal–ligand bonds (assuming idealised symmetry with 90° bond angles), then we have Cu(1)–N(21), Cu(1)–N(31) and Cu(1)–O(1) as the axes. The first of these axes is co-parallel with the equivalent axis on the other three metal centres, but the other two axes are rotated by 90° on moving from one metal centre to the next and therefore interchange. It therefore is reasonable that in a coupled system the g value corresponding to the Cu(1)–N(21) axis at each site is unique, whereas the other two would be averaged and therefore equivalent. This accounts for the appearance of an axial spectrum and for the magnitudes of the g values. Similar g values, but associated with a much larger zero field splitting, were previously observed for a tetranuclear triazolato bridged copper(II) complex.²⁶ The present values seem to be closer to the dipolar contribution.

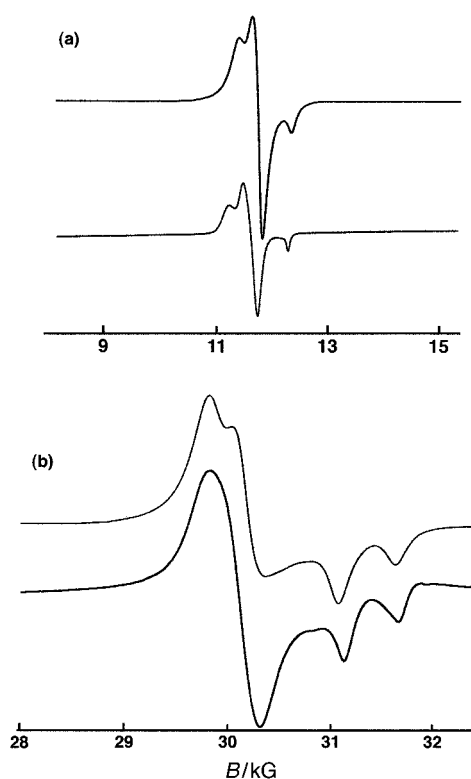


Fig. 12 Experimental (lower line) and simulated (upper line) EPR spectra of $[\text{Cu}_4(\text{L}^2)_4][\text{PF}_6]_4$ under the following conditions: (a) powder spectrum, Q-band, 20 K; (b) powder spectrum, W-band, 25 K.

The most surprising feature of the spectra of both complexes is that they are dominated by a triplet state; there is no unambiguous evidence of the expected quintet state which, given the values of J , we would expect to be thermally populated except at extremely low temperatures. However, there is the feature marked * in the spectra of $[\text{Cu}_4(\text{L}^1)_6][\text{PF}_6]_2$ (Figs. 8 and 10) which is unaccounted for by the simulations. This feature is not due to solid-state effects since it is present in the frozen solution spectra at 100 K; also, it is not due to monomeric impurities since its intensity decreases with decreasing temperature, the reverse of what would be expected from a monomeric centre. The temperature variation of the relative intensity of this feature suggests that it could belong to a spin state which is at a higher energy than the spin-triplet state, *i.e.* it could be from the expected spin quintet. This situation is analogous to that reported by Chaudhuri *et al.*²⁷ wherein they inferred the presence of a spin-quintet state from an analysis of the linewidth and intensity variation with temperature of the X-band powder spectrum of $[\text{Cu}_4\text{L}_4(\text{Im})_4][\text{ClO}_4]_4 \cdot 2\text{H}_2\text{O}$, where L = 1,4,7-triazacyclononane and Im = the imidazolite anion.

Conclusion

The mixed pyridine–pyrazole ligands HL^1 and HL^2 form simple mononuclear octahedral complexes with Ni^{II} and Zn^{II} in which the pyrazole remains protonated. With Cu^{II} however the requirement for an axially elongated geometry precludes this co-ordination mode, with the result that L^1 and L^2 act as anionic bridging ligands *via* deprotonation of the pyrazolate groups to give tetranuclear grid-like complexes in which adjacent copper(II) ions are linked by one or two pyrazolate bridges in various geometries. Variable-temperature magnetic susceptibility studies on these complexes show that (i) there is antiferromagnetic exchange between each pair of adjacent copper(II) ions in every case resulting in $S = 0$ ground states; (ii) the magnitude of the antiferromagnetic exchange depends on

both the number of pyrazolate bridges and the relative orientations of the magnetic orbitals on the copper(II) ions concerned. The EPR spectroscopic measurements at a variety of frequencies and temperatures give spectra characteristic of triplet species, with (in one case) a feature ascribable to the thermally populated quintet state also being apparent.

Acknowledgements

We thank the EPSRC (UK), and Ministero dell'Università e della Ricerca Scientifica e Tecnologia and Consiglio Nazionale delle Ricerche (Italy), for financial support. Miss Claire White is also thanked for assistance with one of the crystal structures.

References

- 1 D. Philp and J. F. Stoddart, *Angew. Chem., Int. Ed. Engl.*, 1996, **35**, 1155; J.-M. Lehn, *Supramolecular Chemistry*, VCH, Weinheim, 1995; C. Piguet, G. Bernardinelli and G. Hopfgartner, *Chem. Rev.*, 1997, **97**, 2005.
- 2 T. Beissel, R. E. Powers and K. N. Raymond, *Angew. Chem., Int. Ed. Engl.*, 1996, **35**, 1084.
- 3 A. J. Amoroso, A. M. W. Cargill Thompson, J. P. Maher, J. A. McCleverty and M. D. Ward, *Inorg. Chem.*, 1995, **34**, 4828; V. A. Ung, A. M. W. Cargill Thompson, D. A. Bardwell, D. Gatteschi, J. C. Jeffery, F. Totti and M. D. Ward, *Inorg. Chem.*, 1997, **36**, 3447.
- 4 M. D. Ward, *Chem. Soc. Rev.*, 1995, 121.
- 5 O. Kahn, *Molecular Magnetism*, VCH, Weinheim, 1993.
- 6 V. A. Grillo, Z. Sun, K. Folting, D. N. Hendrickson and G. Christou, *Chem. Commun.*, 1996, 2233; V. A. Grillo, M. J. Knapp, J. C. Bollinger, D. N. Hendrickson and G. Christou, *Angew. Chem., Int. Ed. Engl.*, 1996, **35**, 1818; H. J. Eppley, H.-L. Tsai, N. de Vries, K. Folting, G. Christou and D. N. Hendrickson, *J. Am. Chem. Soc.*, 1995, **117**, 301; M. A. Bolcar, S. M. J. Aubin, K. Folting, D. N. Hendrickson and G. Christou, *Chem. Commun.*, 1997, 1485.
- 7 Other examples of 'molecular grids': P. N. W. Baxter, J.-M. Lehn, J. Fischer and M.-T. Youinou, *Angew. Chem., Int. Ed. Engl.*, 1994, **33**, 2284; P. N. W. Baxter, J.-M. Lehn, B. O. Kneisel and D. Fenske, *Chem. Commun.*, 1997, 2231; *Angew. Chem., Int. Ed. Engl.*, 1997, **36**, 1978; G. S. Hanan, D. Volkmer, U. S. Schubert, J.-M. Lehn, G. Baum and D. Fenske, *Angew. Chem., Int. Ed. Engl.*, 1997, **36**, 1842; C. Duan, Z. Liu, X. You, F. Xue and T. C. W. Mak, *Chem. Commun.*, 1997, 381.
- 8 V. C. M. Smith and J.-M. Lehn, *Chem. Commun.*, 1996, 2733.
- 9 V. P. Hanot, T. D. Robert, J. Kolnaar, J. G. Haasnoot, J. Reedijk, H. Kooijman and A. L. Spek, *J. Chem. Soc., Dalton Trans.*, 1996, 4275 and refs. therein.
- 10 (a) T. Otieno, S. J. Rettig, R. C. Thompson and J. Trotter, *Inorg. Chem.*, 1995, **34**, 1718; (b) J. Casabó, J. Pons, K. S. Siddiqi, F. Teixidor, E. Molins and C. Miravittles, *J. Chem. Soc., Dalton Trans.*, 1989, 1401; (c) J. Pons, X. López, J. Casabó, F. Teixidor, A. Caubet, J. Ruis and C. Miravittles, *Inorg. Chim. Acta*, 1992, **195**, 61; (d) J. Pons, F. J. Sánchez, A. Labarta, J. Casabó, F. Teixidor and A. Caubet, *Inorg. Chim. Acta*, 1993, **208**, 167; (e) M. Munakata, L. P. Wu, M. Yamamoto, T. Kuroda-Sowa, M. Maekawa, S. Kawata and S. Kitagawa, *J. Chem. Soc., Dalton Trans.*, 1995, 4099; (f) P. M. Slangen, P. J. van Koningsbruggen, K. Goubitz, J. G. Haasnoot and J. Reedijk, *Inorg. Chem.*, 1994, **33**, 1121.
- 11 J. C. Jeffery, P. L. Jones, K. L. V. Mann, E. Psillakis, J. A. McCleverty, M. D. Ward and C. M. White, *Chem. Commun.*, 1997, 175.
- 12 A. J. Amoroso, A. M. W. Cargill Thompson, J. C. Jeffery, P. L. Jones, J. A. McCleverty and M. D. Ward, *J. Chem. Soc., Chem. Commun.*, 1994, 2751; H. Brunner and T. Scheck, *Chem. Ber.*, 1992, **125**, 701.
- 13 J. S. Fleming, E. Psillakis, S. M. Couchman, J. C. Jeffery, J. A. McCleverty and M. D. Ward, *J. Chem. Soc., Dalton Trans.*, 1998, 537.
- 14 P. L. Jones, A. J. Amoroso, J. C. Jeffery, J. A. McCleverty, E. Psillakis, L. H. Rees and M. D. Ward, *Inorg. Chem.*, 1997, **36**, 10.
- 15 SHELXTL 5.03 program system, Siemens Analytical X-Ray Instruments, Madison, WI, 1995.
- 16 D. Gatteschi and L. Pardi, *Gazz. Chim. Ital.*, 1993, **123**, 231.
- 17 W. H. Press, B. P. Flannery, S. A. Teukolsky and W. T. Vetterling, *Numerical Recipes*, Cambridge University Press, 1968.
- 18 G. M. Smith, J. C. G. LeSurf, R. H. Mitchell and P. C. Riedi, *MTT Symposium Proceedings, Orlando*, 1995, *Rev. Sci. Instrum.*, 1998, **69**, 3924.
- 19 F. E. Mabbs and D. Collison, *Electron paramagnetic resonance of d-transition metal compounds*, Elsevier, Amsterdam, 1992, Chs. 7 and 16.
- 20 P. L. Jones, J. C. Jeffery, J. A. McCleverty and M. D. Ward, *Polyhedron*, 1997, **16**, 1567.
- 21 K. Singh, J. R. Long and P. Stavropoulos, *J. Am. Chem. Soc.*, 1997, **119**, 2942.
- 22 W. R. Thiel and T. Priermeier, *Angew. Chem., Int. Ed. Engl.*, 1995, **34**, 1737; W. R. Thiel, M. Angstl and T. Priermeier, *Chem. Ber.*, 1994, **127**, 2373; J. Sieler and H. Hennig, *Z. Anorg. Allg. Chem.*, 1971, **381**, 219; Y. Luo, P. G. Potvin, Y.-H. Tse and A. B. P. Lever, *Inorg. Chem.*, 1996, **35**, 5445.
- 23 G. Eaton and M. C. R. Symons, *J. Chem. Soc., Faraday Trans. 1*, 1988, **84**, 3459.
- 24 D. A. Bardwell, J. C. Jeffery and M. D. Ward, *Inorg. Chim. Acta*, 1995, **236**, 125 and refs. therein.
- 25 V. C. M. Smith and J.-M. Lehn, *Chem. Commun.*, 1996, 2733.
- 26 A. Bencini, D. Gatteschi, C. Zanchini, J. G. Haasnoot, R. Prins and J. Reedijk, *J. Am. Chem. Soc.*, 1987, **109**, 2926.
- 27 P. Chaudhuri, I. Karpenstein, M. Winter, M. Lengen, C. Butzlaff, E. Bill, A. X. Trautwein, U. Flörke and H.-J. Haupt, *Inorg. Chem.*, 1993, **32**, 888.

Paper 8/07599I